ACS APPLIED MATERIALS & INTERFACES

December 4, 2019
Volume 11
Number 48
pubs.acs.org/acsami

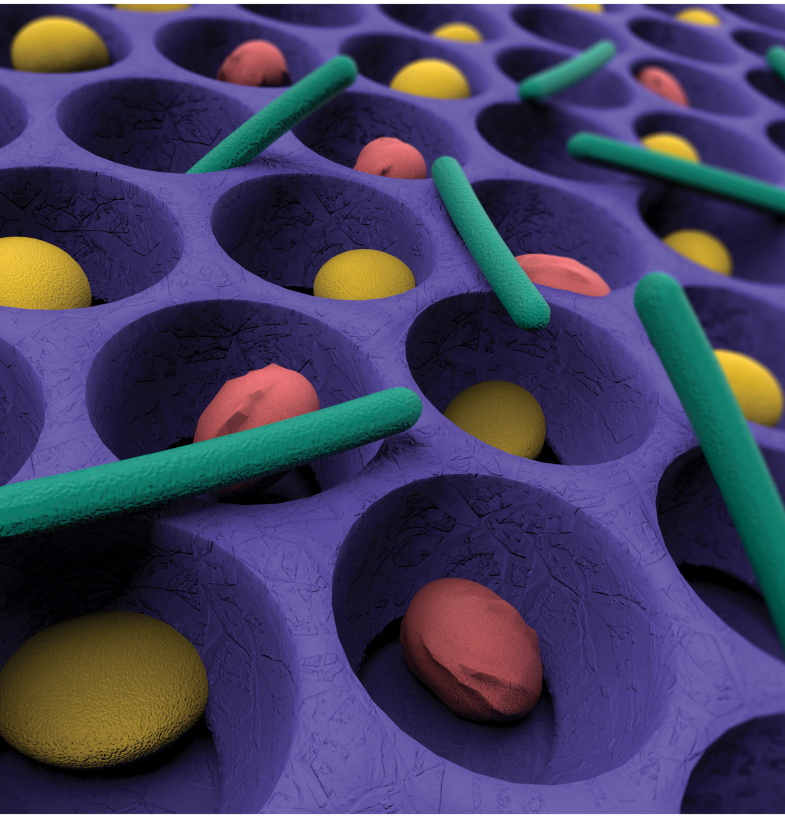

ACS Publications
Most Trusted. Most Cited. Most Read.

www.acs.org

ACS APPLIED MATERIALS & INTERFACES

Research Article

Cite This: ACS Appl. Mater. Interfaces 2019, 11, 44933−44940

www.acsami.org

High-Throughput Identification and Screening of Single Microbial Cells by Nanobowl Array

Xiuyan Li,[†,¶] Hongqing Feng,[‡,∥,¶] Zhe Li,[‡,∥,¶] Yue Shi,[†] Jingjing Tian,[‡,∥] Chaochao Zhao,[‡,∥] Min Yu,[§] Zhuo Liu,[‡] Hu Li,[‡] Bojing Shi,[‡] Qian Wang,[†] Luhai Li,[†] Dongshu Wang,[#] Li Zhu,*[,#] Ruping Liu,*[,†] and Zhou Li*[,‡,∥,⊥]

[†]Beijing Institute of Graphic Communication, Beijing 102600, P. R. China

[‡]CAS Center for Excellence in Nanoscience, Beijing Key Laboratory of Micro-nano Energy and Sensor, Beijing Institute of Nanoenergy and Nanosystems, Chinese Academy of Sciences, Beijing 100083, P. R. China

[∥]School of Nanoscience and Technology, University of Chinese Academy of Sciences, Beijing 100049, P. R. China

[§]School of Stomatology and Medicine, Foshan University, Foshan 528000, P. R. China

[⊥]Center on Nanoenergy Research, School of Physical Science and Technology, Guangxi University, Nanning 530004, P. R. China

[#]State Key Laboratory of Pathogen and Biosecurity, Beijing Institute of Biotechnology, Beijing 100071, P. R. China

Supporting Information

ABSTRACT: High-throughput screening and fast identification of single bacterial cells are crucial for clinical diagnosis, bioengineering, and fermentation engineering. Although single-cell technologies have been developed extensively in recent years, the single-cell technologies for bacteria still need further exploration. In this study, we demonstrate an identification and screening technology for single bacterial cells based on a large-scale nanobowl array, which is well-ordered and size-adjustable for use with different kinds of bacteria. When the culture medium with monodispersed bacteria was placed on the nanobowl array, it successfully enabled loading of single bacterium into a single nanobowl. Because of the limitative size and depth of the nanobowls, mixture of different bacteria species could be screened according to their sizes. In addition, with the help of a low electrical current, the bacteria can be further screened according to their intrinsic surface charges. If combined with micromanipulation technology, high-throughput single bacterial selection can be achieved in future.

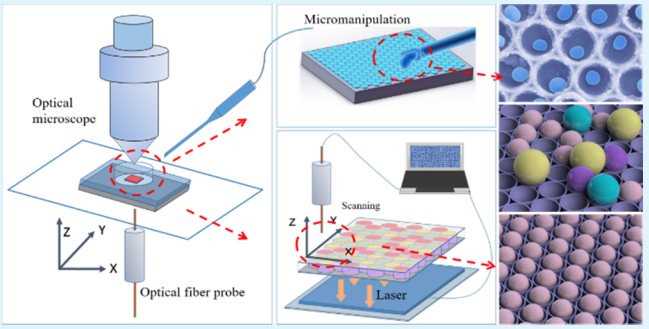

KEYWORDS: *nanobowl array, high-throughput screening, bacteria, single-cell identification, surface charges*

INTRODUCTION

Analysis of colonies at the single-cell level with high-throughput identification and screening technology is highly demanded in many biological applications, such as selection of improved industrial microorganisms,[1,2] screening of antimicrobial drugs,[3,4] clinical sample diagnosis,[5,6] and microbiological genetics.[7,8]

Many single-cell technologies have been developed in the past decades,[9] including fluorescence-activated cell sorting (FACS),[10,11] microfluidics, microwell arrays,[12,13] microcontact printing,[14,15] and single-cell microscopy technologies.[16] Single-cell sequencing is also a very hot research field.[17,18] FACS realizes single-cell isolation with the help of sheath fluid, and the single-cell analysis is based on specific fluorescent antibodies toward certain markers of the cells.[10] Microfluidics employs laminar and droplet technologies to strictly control the flow rate of the cell solution and achieves single-cell isolation with the help of microchannels and droplets.[19,20] Microfluidics requires precise device fabrication and sophisticated fluid control.[21,22] In the microcontact printing technology, the bacterial liquid is patterned into a microporous structure for bacterial dispersion and identification. However, it is difficult to separate a single cell by the pattern printing method.[15] Single-cell microscopy technologies make it possible to observe a single cell or a small bacteria cluster in details, but they cannot do the observation in a high-throughput way.[23,24] Single-cell sequencing is highly welcome in biological research studies, because it can disclose the genetic information of a special single cell, which will otherwise be covered by those of the large cell population. However, the isolation of single cells has to be done via FACS or microfluid technologies.

Received: May 23, 2019
Accepted: November 1, 2019
Published: November 1, 2019

DOI: 10.1021/acsami.9b08662
ACS Appl. Mater. Interfaces 2019, 11, 44933−44940

Single-cell arrays to trap an individual cell in their wells have specific advantages because each "spot" can be an individual cell, and the regularly arranged "spot" can align each cell with precise location.[25,26] Liu et al. fabricated a micro-well array to retain both adherent and nonadherent cells with high efficiency.[27] Ueda et al. created a droplet microarray with thousands of isolated microdroplets, which have defined geometry and volume, and prepared a high-density array of hydrogel micropads encapsulating live cells.[13] Yamamura et al. described a single-cell microarray system to analyze cellular response of individual cells such as lymphocytes.[28] Basically, the studies of single-cell arrays based on mammalian cells are more than the microbial cells, because the microbial cells are much smaller, and the difficulty to load single microbial cells in the arrays is much larger than mammalian cells. Usually, the loading of microbial cells into arrays is carried out with the help of microfluidics, micropillars, or micromagnet arrays.[29,30]

In the present work, a low-cost, efficient, and easy to operate method to do single-cell microorganism identification and screening was developed based on a nanobowl array. A large-area, well-ordered nanobowl array was fabricated on indium tin oxide (ITO) wafers.[31−33] Monodispersed bacteria were loaded into the nanobowl array, which enabled the formation of a single-cell array with one bacterial cell per nanobowl. Various fluorescent microspheres and mixtures of various bacteria cells were loaded into the nanobowl arrays and identified. With the help of a low electrical current, the nanobowl array can in further realize the bacteria cell screening based on their surface charges. This work enabled a simple, accurate, and high-throughput way to identify and screen bacteria cells.

RESULT AND DISCUSSION

Characterization of the Nanobowl Array. Following the fabrication procedure, a close-packed monolayer of polystyrene (PS) microspheres with a diameter of 2 μm was assembled on the ITO substrate (Figure 1a and Figure S1a−c).[31−33] Figure S2a−cshows the formation of a white large-area single-layer PS microsphere membrane on the ITO wafers. After Al_2O_3 coating, inductively coupled plasma (ICP) etching, and PS microsphere dissolving, a close-packed and high-ordered Al_2O_3 nanobowl array was formed on the substrate (Figure S2d). Figure 1b,c shows the top-down and tilted scanning electron microscopy (SEM) images of the nanobowl structure, respectively. In Figure 1d, a low-magnification SEM image of the nanobowl array indicates that a large-area array was formed. There was a transparent hole at the center bottom of each nanobowl, exposing the ITO substrate (Figure 1e and Figure S2e). This is because the PS microspheres adhered closely to the ITO substrate, and those attached area were not coated with Al_2O_3.[34] Therefore, the center bottom of each nanobowl was transparent, allowing transmitted optical observation. As shown in Figure 1f, both transmitted light and reflected light could enter the nanobowls. Figure 1g,h shows the transmission and reflection images, respectively, which verify the presence of the transparent bottom holes. We also used microspheres with other diameters as the template to fabricate the nanobowl arrays (Figure 1i,l). The detailed characteristics of different nanobowl arrays are listed in Tables 1 and 2. Each data was obtained from measurements of 45 nanobowls (15 nanobowls × 3 independent arrays). The wall thickness of various nanobowl arrays differed from each other (Table 1). In addition, the ALD cycles also had impact on the wall thickness (Table 2). The dimensions of the transparent

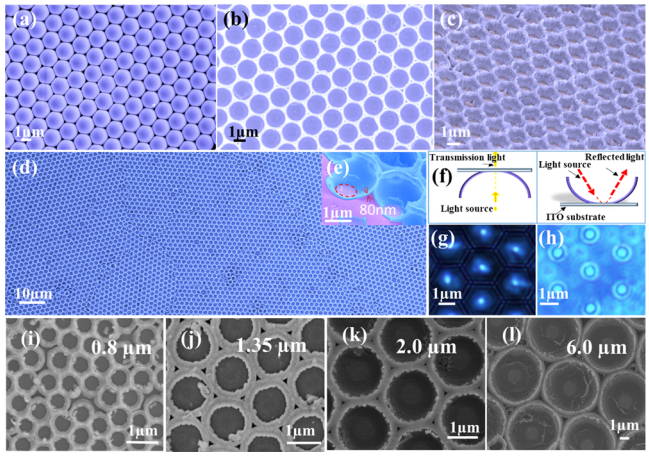

Figure 1. Formation and structural characteristics of the nanobowl array. (a) The SEM images of close-packed PS microspheres array. (b) Top-down and (c) tilted SEM images of the nanobowl structure. (d) Low-magnification SEM image of the nanobowl array. (e) The SEM image of transparent holes at the bottom center of each nanobowl. (f) Schematic of transmitted light and reflected light due to the transparent holes at the center of each nanobowl. Optical image of (g) transmitted light and (h) reflected light with structural characteristics of the nanobowl. Diameter of microspheres: 2 μm. (i−l) Different nanobowl arrays made from microspheres with different diameters.

holes of the nanobowls made from 2 μm microspheres were also measured, which were 271.2 ± 30.4 nm.

Fluorescent Microsphere Loading in the Nanobowl Array. Figure 2a shows the fluorescence microscopy (FM) images of the nanobowl array with green fluorescent microspheres trapped in the bowls. The inset of Figure 2a is a high-magnification SEM image of the nanobowl array loaded with microspheres—there was an almost perfect match of one-ball one-bowl. These results show that the nanobowl array enabled quick and accurate preparation of a fluorescent microsphere array. With the aid of confocal microscopy, we can effectively locate a single fluorescent microsphere on a large-scale substrate loaded with millions of microspheres.

Next, we loaded the nanobowl array with a mixture of fluorescent microspheres of two colors (Figure 2b−f). Because the fluorescent microspheres were highly ordered as trapped in the nanobowl array, it could be observed that green and red fluorescent microspheres were well distinguished in one array (Figure 2b,c). In addition, mixed fluorescent microspheres could be screened and identified in the ordered nanobowl array. The merged image of the fluorescent and the bright field images shows that the one-ball in one-bowl discipline worked well here (Figure 2d−f). Next, we extended this approach to screen real bacterial cells.

Bacteria Loading in the Nanobowl Array. *Staphylococcus aureus* (*S. aureus*) cells were first loaded into the nanobowl array to demonstrate bacterial identification and screening. The loading of bacteria is much more difficult than the microspheres because the bacteria grow in bunches with strong surface adhesions between one another. In this study, we established a method to effectively monodisperse *S. aureus* cells. By using trypsin, ultrasonic treatment, and control of the growth stage, highly monodispersed *S. aureus* cell solution could be prepared before loading and most of the nanobowl contained one bacteria each.

DOI: 10.1021/acsami.9b08662
ACS Appl. Mater. Interfaces 2019, 11, 44933−44940

Table 1. Wall Thickness and Inner Diameters of the Nanobowls Made from Different Microspheres (n = 45, from 15 Nanobowls × 3 Independent ITO Substrates)

diameter of the microspheres (μm)	0.80	1.35	2.00	6.00
wall thickness of nanobowls (nm)	93.0 ± 9.6	169.7 ± 11.9	131.9 ± 12.7	83.2 ± 7.6
inner diameter of nanobowls (μm)	0.56 ± 0.02	1.06 ± 0.04	1.64 ± 0.05	5.26 ± 0.24

Table 2. Wall Thickness of the Nanobowls Made from 2.0 μm Microspheres, after Different ALD Cycles (n = 45, from 15 Nanobowls × 3 Independent ITO Substrates)

ALD cycles	400	800
wall thickness of nanobowls (nm)	131.9 ± 12.7	231.9 ± 32.19

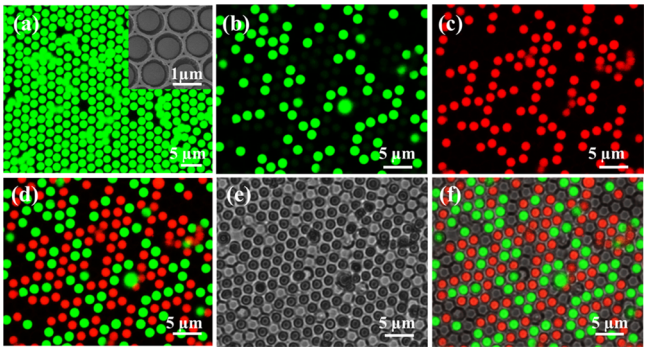

Figure 2. FM, SEM, and bright field images of ordered microsphere array located in nanobowls. (a) FM image of ordered green fluorescent microspheres located in nanobowls. Inset: High-magnification SEM image of the fluorescent microsphere array. (b, c) FM images of the green and red fluorescent microspheres loaded in one nanobowl array. (d) The merged image of (b) and (c). (e) Bright field image of the nanobowl array loaded with microspheres. (f) Merged image of (d) and (e).

Fluorescent array images of live bacteria are shown in Figure 3a,b. Figure 3a,b shows the arrangement of *S. aureus* with different seeding times; the data indicate good dispersity and identification of the *S. aureus* in the ordered nanobowl array. Figure 3c shows that *S. aureus* cells were uniformly dispersed in the nanobowls. Figure 3d shows that the occupation fraction of the nanobowls for *S. aureus* changed with the sedimentation time. The occupation proportion was calculated from these images for different seeding times using the following expressions

$$w(\%) = \frac{n_1}{n_0} \quad (1)$$

where n_1 and n_0 denote the number of nanobowl loaded with bacteria and the total number of nanobowl, respectively. When the sedimentation time reached 4 h, the occupation fraction stopped going higher. Figure S4 shows specifically the fluorescent *S. aureus* images at different sedimentation times when the *S. aureus* concentrations were all 8.0×10^8 cells/mL. These results all suggested that a seeding time of 4 h was sufficient. The cell capture ratio by the nanobowl array was 93.2 ± 4.8% and the single-cell capture ratio was 82.7 ± 5.8% (n = 600, 200 nanobowls × 3 ITO substrates; Figure S3a). Figure S3b shows that occasionally there were more than one *S. aureus* cell in a single nanobowl, perhaps because they were not fully monodispersed. We also tried other cell densities. At a density of 8×10^7 cells/mL, the cell capture ratio reduced to 44.4 ± 5.6%. At a density of 8×10^6 cells/mL, the cell capture

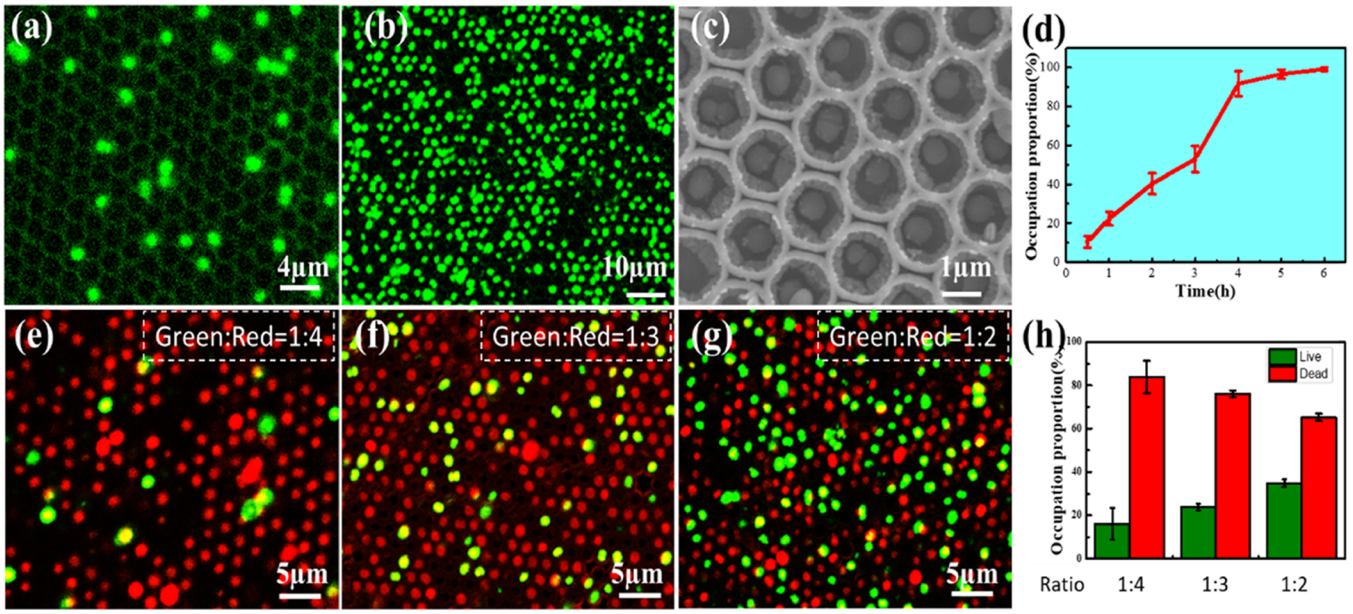

Figure 3. Images of *S. aureus* in the nanobowl array with different sedimentation times and different ratios of live and dead bacteria. (a, b) FM image of live *S. aureus* stained green, and the sedimentation times were 1 and 4 h. (c) SEM image of *S. aureus* trapped in the nanobowls. (d) The occupation fraction of the nanobowls by *S. aureus* changed with the sedimentation time. Error bars represent ±SD. (e–g) FM images of live and dead mixed *S. aureus* cells; the mixture ratios of green (live) and red (dead) bacterial cells were 1:4, 1:3, and 1:2. (h) Nanobowl occupation proportion of live and dead *S. aureus* mixed at ratios of 1:4, 1:3, and 1:2. Error bars represent ±SD.

DOI: 10.1021/acsami.9b08662
ACS Appl. Mater. Interfaces 2019, 11, 44933–44940

ratio reduced to 0 and none of the cells was loaded into the nanobowls. Why the cell density has such marked impact on the capture ratio still needs further investigation.

To further study the screening of bacteria in the nanobowl array, we tried to load a mixture of live and dead *S. aureus* onto the nanobowls. We found that both the dead bacteria and live bacteria can form large-area-ordered single-cell arrays on the nanobowl array (Figure S5). A series of experiments were conducted with different ratios of live and dead bacteria, which were respectively stained by SYTO 9 (green) and propidium iodide (PI, red). Mixtures of live and dead *S. aureus* cells were prepared at ratios of 1:2, 1:3 and 1:4. Figure 3e–g shows the fluorescence images for each mixture ratio seeded on the nanobowl array. The nanobowl occupation proportion for live and dead *S. aureus* was very accordant with the ratio in the mixture applied to the array (Figure 3h). The data are shown in Table 3 (n = 600, 200 nanobowls × 3 ITO substrates), which demonstrated the accordance.

Table 3. Ratio of Live and Dead Cells in the Original Mixture and on the Nanobowl Arrays

mixed ratio (green:red)	1:4	1:3	1:2
counted green ratio	0.18 ± 0.06	0.24 ± 0.01	0.34 ± 0.02
counted green ratio	0.82 ± 0.06	0.76 ± 0.01	0.66 ± 0.02
counted ratio (green:red)	1:4.5	1:3.2	1:1.9

Also, the bacteria were loaded into the nanobowls complying with the one in one discipline. As shown in Figure S6a–c, live and dead bacteria were seeded in the nanobowls in a regularly ordered arrangement. We drew lines on Figure S6c according to the alignment of the nanobowl array, as shown in Figure S6d. There was one single fluorescent bacteria cell per nanobowl, which meant that a single *S. aureus* cell was loaded in an individual nanobowl.

Bacterial Identification and Screening Using the Nanobowl Array. To determine whether the nanobowl array could be used for identification and screening of other bacterial species, we tried its ability to load *Escherichia coli* (*E. coli*),[13] *Streptococcus suis* (*S. suis*),[35] *Shigella flexneri* (*S. flexneri*),[36] and dormant bacteria *Bacillus anthracis* (*B. anthracis*) spores.[37] *B. anthracis* is responsible for the zoonosis anthrax, which causes serious diseases and was used in bioterrorism incidents. *B. anthracis* is mostly present in the form of dormant spores in the environment. Anthrax infection occurs via introduction of *B. anthracis* spores into a skin abrasion, inhalation, or ingestion. Therefore, the detection of spores is very important.[38] *S. suis*, which is very harmful to the aquaculture industry and employees, is an important swine pathogen and can infect humans. It can cause meningitis, septicaemia, endocarditis, arthritis, and septic shock.[35] *S. flexneri*, as a serotype of *Shigella* bacteria, could cause shigellosis, which is one of the most common diarrheal intestinal diseases worldwide. With consistently high incidence rates and the emergence of multidrug-resistant *Shigella* strains, shigellosis is a critically important global health problem.[39]

As shown in Figure 4a–h and Figure S8, *B. anthracis* spores and short rod-shaped *S. flexneri* cells were successfully loaded into the nanobowls, one bacterium in one bowl (Figure 4a,b,e,f). For *E. coli* cells, which are longer and slimmer than *S. flexneri* cells, there are two kinds of orientation states: horizontally and vertically. This is coordinate with Sarangi et al.'s work[40] in which they also reported both vertical and

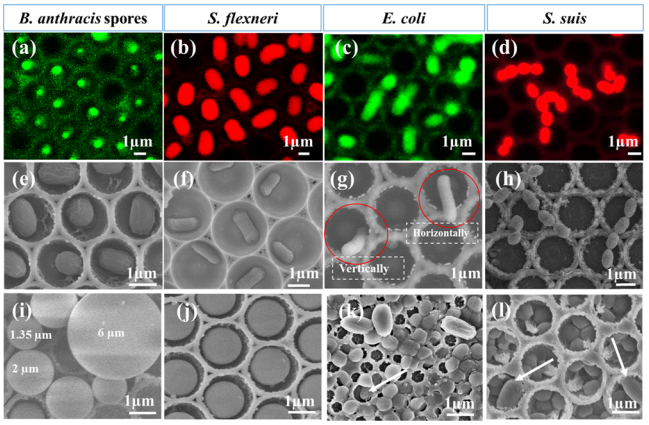

Figure 4. (a–h) Various bacteria loaded into the nanobowl array: (a, e) *B. anthracis* spores, (b, f) *S. flexneri*, (c, g) *E. coli*, (d, h) *S. suis*. (i) Mixture of microspheres was loaded with the nanobowl array. The diameters of microspheres were 1.35, 2, and 6 μm. (j) Microspheres with a diameter of 1.35 μm were loaded into the 2 μm nanobowls. (k) Mixture of *S. aureus* cells and *B. anthracis* spores was loaded with the 800 nm nanobowl array: none of them could be loaded; only one *S. aureus* cell was loaded into a nanobowl, which had a much larger diameter (white arrow). (l) Mixture of *S. aureus* cells and *B. anthracis* spores was loaded with the 2 μm nanobowl array: both of them were loaded, even within the same nanobowl (white arrows).

horizontal orientations of *E. coli* bacteria cells on an InP nanowire array. The horizontally orientated *E. coli* cells cannot be fully loaded into the nanobowls because their longside cell body has exceeded the diameter of the nanobowls. If vertically orientated, the *E. coli* cells will be loaded in an inserted way (Figure 4c,g). However, the peanut-shaped (*S. suis*) bacteria could not seed into nanobowls because they could not be monodispersed (Figure 4d,h). The results of the above experiments indicate that it is possible to achieve the identification and screening of single cells of many bacteria using the nanobowl array in a size-sensitive way. Because the *S. suis* cells were not monodispersed, the overall size of a cell cluster was larger than the size of the nanobowl. Therefore, *S. suis* could not be loaded.

To confirm the size-sensitive loading property of the nanobowl array, mixtures of microspheres and bacteria were applied. The microspheres with diameters of 1.35, 2, and 6 μm were applied (Figure 4i). The mixed microspheres were added into a mixture of 50 μL of ethanol and 100 μL of deionized water to form a 0.5% suspension. The suspension was placed on the nanobowl array and the seeding duration was 1 h. The microspheres with a diameter of 1.35 μm fell perfectly into the nanobowls, but the others did not (Figure 4j). It suggested that only the microparticles with a diameter of <2 μm could fall into the 2 μm nanobowls.

Next, the mixture of *S. aureus* cells and *B. anthracis* spores was placed on the nanobowl array for loading. When loaded with the 800 nm nanobowl array, none of them could be loaded because their sizes all exceeded 800 nm at any dimension (Figure 4k). Only one *S. aureus* cell was loaded into a nanobowl, because that bowl had a much larger diameter (white arrow). When loaded with the 2 μm nanobowl array, both of the cells and spores were loaded, even within the same nanobowl (white arrows). These results demonstrated that the nanobowl array could identify and screen the bacteria mixture depending on their sizes.

DOI: 10.1021/acsami.9b08662
ACS Appl. Mater. Interfaces 2019, 11, 44933–44940

Electrical Current Enhances the Screening Ability of Nanobowl Array. Because the nanobowl substrate ITO was electrically conductive, the influence of electrical current on the screening ability of the nanobowl array was investigated. The setup of the electrical current application is illustrated in Figure 5a. Without the electrical current, only a few *S. aureus*

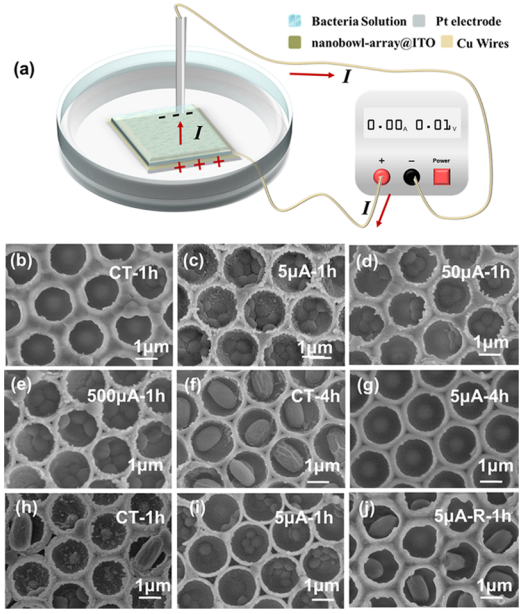

Figure 5. Enhanced screening ability of the nanobowl arrays with the help of electrical current. (a) The schematics of the electrical current application on the nanobowl array. (b) A few *S. aureus* cells were loaded into the nanobowls after 1 h without electricity, and some other cells landed on the edges of the nanobowls. (c–e) Many *S. aureus* cells were loaded into the nanobowls after 1 h with (c) 5 μA current, (d) 50 μA current, and (e) 500 μA current. (f) Many *B. anthracis* spores were loaded into the nanobowls after 4 h natural sedimentation. (g) None of the *B. anthracis* spores was loaded into the nanobowls after 4 h with 5 μA current. (h) Both the *S. aureus* cells and *B. anthracis* spores were loaded without the current. (i) Many *S. aureus* cells were loaded but none of the *B. anthracis* spores was loaded with 5 μA current. (j) When the electrical current flow was reversed, many *B. anthracis* spores were loaded into the nanobowls after 1 h with 5 μA current but not the *S. aureus* cells.

cells were loaded into the nanobowls after 1 h, and some cells had just landed on the edges of the nanobowls (Figure 5b). With the help of 5 μA current, many *S. aureus* cells were trapped into the nanobowls. The attraction effect was so strong that most of the nanobowls captured more than one *S. aureus* cell (Figure 5c). This is because the *S. aureus* cells have negative surface charges.[41,42] When the applied current increased to 50 and 500 μA, the loaded cells did not increase very much (Figure 5d,e), suggesting that 5 μA current was enough to induce the accelerated loading of *S. aureus* cells. The situation was completely opposite for the *B. anthracis* spores, because the spores have positive surface charges. After 4 h natural sedimentation, the *B. anthracis* spores were fully loaded into the nanobowls (Figure 5f). If electrial current was applied, none of the spores could be loaded into the nanobowls: the nanobowl completely repelled the spores (Figure 5g). When the mixture of *S. aureus* cells and *B. anthracis* spores was loaded with the nanobowl array, the results were consistent with before. Both of them could be loaded into the nanobowls via natural sedimentation after 1 h (Figure 5h), although the loading ratio was low. If the 5 μA current was applied, much more *S. aureus* cells would be loaded, but none of the *B. anthracis* spores would (Figure 5i). We also managed to trap the *B. anthracis* spores in the nanobowls instead of the *S. aureus* cells by reversing the electrical current direction and making the ITO substrate negative and the Pt needle positive. As shown in Figure 5j, after the current direction was reversed, many *B. anthracis* spores were loaded into the nanobowls after 1 h with 5 μA current but not the *S. aureus* cells.

Perspectives. This nanobowl array can be adopted for high-throughput identification and screening of single microbial cells, whether in single species or multiple microorganisms. The ordered nanobowl array can accurately encode an array of cells to achieve the identification and screening of single cells of different sizes. In addition, the nanobowl array can screen the bacteria cells according to their surfaces with the help of a low electrical current. This technology has the potential to impact a range of applications in the laboratory and clinical diagnosis.[43,44] With an advanced high-power microscope and micromanipulation technology, research on the single-cell level could be developed based on this ordered single-cell array. Figure 6a illustrates a perspective of a fiber optic scan system

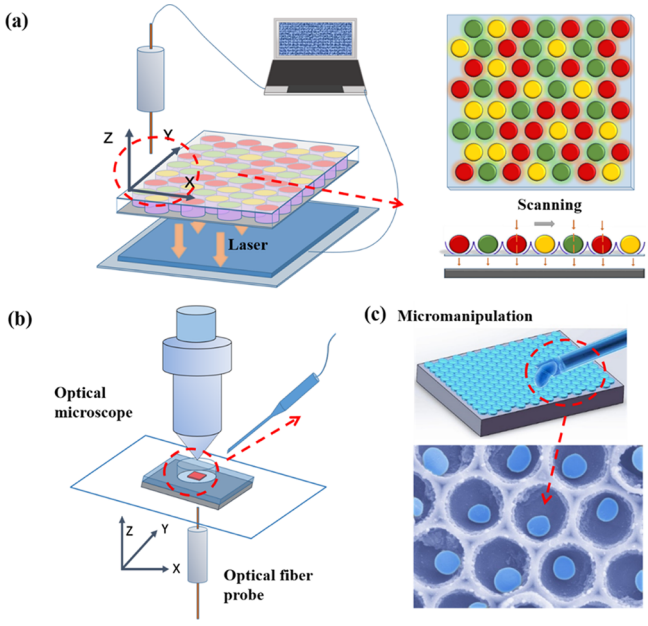

Figure 6. Application of the nanobowl array to identification and screening of bacteria. (a) Schematic illustration of fiber optic scanning processing of the nanobowl array. (b, c) Schematic illustration of a fiber optic scan system integrated with the micromanipulation technology.

integrated with the single-cell bacterial array, which can scan fluorescence to code the position of fluorescent bacteria. Micromanipulation of single cells might become possible in single-cell analysis with the aid of identification and screening of single bacterial cells (Figure 6b,c). Additionally, this technology has potential applications in the information-access process of reporter strains.

CONCLUSIONS

In this study, a technique is developed for high-throughput identification and screening of bacteria using a nanobowl array. The nanobowl structure shows excellent optical and structural

DOI: 10.1021/acsami.9b08662
ACS Appl. Mater. Interfaces 2019, 11, 44933−44940

Table 4. Bacteria Used in This Study

bacterial strains	shape	size (μm)	fluorescence	note
B. anthracis A16DD[1]	ellipse-shaped	0.8 × 1.2−1.7	green fluorescent protein (GFP)	spore-forming Gram-positive bacteria, avirulent strain, two virulence plasmid-cured
S. flexneri 301 ΔpCP	short rod-shaped	0.7 × 1−3	mScarlet	Gram-negative bacteria, avirulent strain, the virulence plasmid-cured
S. suis	peanut-shaped	0.5−2.0	PI	Gram-positive bacteria, wild-type strain
S. aureus	grape-shaped	0.8−1.5	PI/SYTO 9	Gram-positive bacteria, avirulent strain, wild-type strain
E. coli	short rod-shaped	0.5 × 1−3	SYTO 9	Gram-negative bacteria, avirulent strain,

properties. High-throughput experimentation with single bacterial cells and microspheres provides proof of principle that the nanobowl array has the ability to identify and screen bacteria of different sizes. In addition, the nanobowl array can screen the bacteria cells according to their surface charges with the help of a low electrical current. This technology is easy to operate and does identification and screening in a high-throughput way. Additionally, in situ detection could be effectively developed with the aid of methods such as atomic force microscopy and Raman spectroscopy.[43,44] The regularly ordered single bacteria in a nanobowl array might be a useful genetic unit to realize coding identification that differs from current microfluidic devices. It shows great potential for wide applications in microbial analysis.

METHODS

Fabrication of the Nanobowl Array. The fabrication procedures are schematically illustrated in Figure S1. First, homogeneous PS microspheres were self-assembled onto an ITO substrate to form an ordered monolayer PS microsphere array (Figure S1a,b). Then, Al_2O_3 was deposited on the surface of the PS microsphere array by atomic layer deposition (ALD) (PICOSUM/SUNALE R-200) (Figure S1c). The pressure of the chamber was set to be 4.5×10^{-3} Torr, the temperature of the reaction chamber was set to be 80 °C, and the outer chamber was set to be 180 °C. $Al(CH_3)_3$ (trimethyl aluminum, TMA) and H_2O were used as precursors, and N_2 (99.9999%) was used as purged gas. The cycle was TMA(100 ms)-N_2(2 s)-H_2O(100 ms)-N_2(8 s). The deposition lasted for 400 or 800 cycles. Then, the Al_2O_3 nanobowl array was formed by doing inductively coupled plasma (ICP) etching (SENTECH/SI 500), which retained the down half of the Al_2O_3 layer (Figure S1d). The pressure was 2 Pa. The ICP power and RF power were 400 and 100 W, respectively. The flow rates of CF_4 and O_2 were 30 and 10 sccm, respectively. The etching time lasted for 5 min. After ICP etching, the samples were ultrasonically washed in toluene for 3 min at 40 W. Then, the residual PS microspheres were removed by soaking the samples in toluene for 2 h, and the nanobowl array was formed. The samples were further ultrasonically washed in ethanol for 2 min at 40 W and then soaked in ethanol for 30 min. Finally, the samples were washed by deionized water and blown dry with nitrogen.

Characterization of the Nanobowl Array. A SEM (SU8050) operated at 10 or 15 kV was used to investigate the morphology of the nanobowl array. FM images were obtained using a laser scanning confocal microscopy (Leica TCS SP8) observed under an oil immersion lens.

Bacterial Culture and Fluorescent Labeling. The bacteria studied in this work are listed in Table 4. The bacteria tested in this study included: spherical shaped (*S. aureus*, *S. suis*, and *B. anthracis* spores) and rod shaped (*S. flexneri* and *E. coli*). They are the representatives of Gram-positive bacteria (*S. aureus* and *S. suis*), Gram-negative bacteria (*S. flexneri* and *E. coli*), and dormant bacteria (*B. anthracis* spores). For observation under the laser scanning confocal microscopy, the fluorescent bacteria were prepared. Inactivated *S. suis* and *S. aureus* were labeled with propidium iodide (PI) to emit red light. *E. coli* and live *S. aureus* were labeled with SYTO9 to emit green light. The *B. anthracis* spores contain a GFP expressing plasmid pBE2-eag-GFP to become green emitting, and *S. flexneri* bacteria contain a RFP expressing plasmid pUC-mScarlet to become red emitting. *S. suis* was cultured in fresh THB broth supplemented with 2 g of yeast extract at 37 °C, 180 r/min for 12 h and then inactivated by adding 4% formaldehyde (1:9) and incubated for 24 h. *S. flexneri* was cultured in LB broth at 37 °C, 225 r/min for 10 h and then centrifuged to collect the bacteria. *B. anthracis* strains were cultured on LB agar plates (LB broth supplemented with 1.2% agar) for 3 days to grow into spores. The culture was resuspended in 10% glycerol and then heated in a water bath at 48 °C for 12 h to fully release the spores. The culture was then centrifuged at 4200 rpm for 10 min at 4 °C. The supernatant was removed and the harvested spores were further purified using the solution that contains 66% diatrizoate meglumine and 10% diatrizoate sodium as previously reported protocols. Purified spores was resuspended in ddH_2O and centrifuged at 8000 r/min for 10 min. The supernatant was removed and this procedure was repeated three times, with endospores being resuspended in a final volume of 5 mL, which was refrigerated at 4 °C.[45]

Formation of Monodisperse Bacteria. The *S. aureus* bacteria cells grow in bunches with strong surface adhesions between one another.[46] Thus, we investigated a detergent-free method to disperse the cells. First, the bacteria cells were collected at a log phase because there were more single cells at that stage. Second, bacterial suspension was treated with trypsin for 3 min, and the dispersion of the bacteria was enhanced after trypsin treatment, because this treatment could eliminate adhesion between bacterial cells. Finally, ultrasonic treatment was applied to help the dispersion of the bacteria cells for 1 min at a power of 40 W.

Fluorescent Microsphere Loading in the Nanobowl Array. As the inner diameter of the nanobowls was approximately 2 μm and *S. aureus* cells are approximately 0.8−1.5 μm in diameter, fluorescent microspheres of a diameter of 1.35 μm were chosen for initial experiments. The concentration of the microsphere suspension was 0.01 wt %; 200 μL of microsphere suspension was added onto the nanobowl array and held for 1 h. Then, the nanobowl arrays were gently rinsed twice using deionized water. Because of surface tension, the microspheres loaded in the nanobowls were not washed away. To avoid aggregation, the microsphere suspension was treated ultrasonically for 1 min at a power of 40 W before loading into the nanobowl array.

Bacterial Cell Loading in the Nanobowls Array. After culture, the microbe cells were harvested and received the monodisperse treatment. Then, they were centrifuged at 6000 rpm for 5 min and resuspended with phosphate-buffered saline (PBS, 0.01 M, pH 7.4; Beijing Solarbio) to reach a concentration of 8.0×10^8 cells/mL. Five hundred microliters of suspension was added to the nanobowl array on the ITO and let them to sediment. The optimum sedimentation time was found to be 4 h at ambient temperature. Then, the nanobowl arrays were gently rinsed twice using deionized water.

Application of Electrical Current on the Nanobowl Array. First, the nanobowl array was deposited with a thin layer of Au to enhance the conductivity of the nanobowls. The ITO substrate was connected to the cathode of a DC power supply via a Cu wire. Five hundred microliters of bacteria solution was placed on the top of the nanobowl array. Then, a Pt needle tip was inserted into the bacteria solution and connected to the anode of the DC power. The current

DOI: 10.1021/acsami.9b08662
ACS Appl. Mater. Interfaces 2019, 11, 44933−44940

(μA) passing through the bacteria solution at different output potentials (V) is listed in Table 5.

Table 5. Current Passing through the Bacteria Solution at Different Output Potentials

potential (V)	0.01	0.1	1
current (μA)	5	50	500

■ ASSOCIATED CONTENT

Supporting Information

The Supporting Information is available free of charge on the ACS Publications website at DOI: 10.1021/acsami.9b08662.

Schematic illustration of the process to fabricate 2D nanobowl arrays and bacteria/fluorescent sphere suspension loading into the nanobowl array; formation and structural characteristics of the nanobowl array; the morphology of PS microspheres with different sizes of microspheres and the same thickness of wall; the distribution of number of *S. aureus* cells per nanobowl as a percentage of the total number of nanobowls after different treatments, the SEM images of 0 cell, 1 cell, 2 cells, 3 cells, and more than 4 cells located in individual nanobowls; efficiency of bacteria cells loading into single nanobowl with the change of time; fluorescent, bright field, and SEM images of bacteria in nanobowl array; fluorescent images of an ordered *S. aureus* array; *B. anthracis* spores seeded in unstructured (PDF)

■ AUTHOR INFORMATION

Corresponding Authors

*E-mail: jewly54@126.com (L.Z.).
*E-mail: liuruping@bigc.edu.cn (R.L.).
*E-mail: zli@binn.cas.cn (Z.L.).

ORCID

Zhou Li: 0000-0002-9952-7296

Author Contributions

¶X.L., H.F., and Z.L. contributed equally to this work.

Notes

The authors declare no competing financial interest.

■ ACKNOWLEDGMENTS

The authors thank the support of National Key R&D project from Minister of Science and Technology, China (2016YFA0202703), National Natural Science Foundation of China (No.61971049, 61875015, 31571006, 81601629, and 21801019), Beijing Natural Science Foundation (2182091), Beijing Municipal Science & Technology Commission (Z181100004418004), the Research and Development Program of BIGC (Ec201808), Science and Technology Planning Project of Guangdong Province (2018B030331001), and the National Youth Talent Support Program.

■ REFERENCES

(1) Hochbaum, A. I.; Aizenberg, J. Bacteria Pattern Spontaneously on Periodic Nanostructure Arrays. *Nano Lett.* **2010**, *10*, 3717−3721.
(2) Zhang, Y.-X.; Perry, K.; Vinci, V. A.; Powell, K.; Stemmer, W. P. C.; Del Cardayré, S. B. Genome Shuffling Leads to Rapid Phenotypic Improvement in Bacteria. *Nature* **2002**, *415*, 644−646.
(3) Mesak, L. R.; Qi, S.; Villanueva, I.; Miao, V.; Davies, J. Staphylococcus aureus Promoter-Lux Reporters for Drug Discovery. *J. Antibiot.* **2010**, *63*, 492−498.
(4) Liu, Y.; Yang, S.-F.; Tay, J.-H. Improved Stability of Aerobic Granules by Selecting Slow-Growing Nitrifying Bacteria. *J. Biotechnol.* **2004**, *108*, 161−169.
(5) Wei, X.; Gao, J.; Wang, F.; Ying, M.; Angsantikul, P.; Kroll, A. V.; Zhou, J.; Gao, W.; Lu, W.; Fang, R. H.; Zhang, L. In Situ Capture of Bacterial Toxins for Antivirulence Vaccination. *Adv. Mater.* **2017**, *29*, 1701644.
(6) Zhang, W.; Guo, S.; Pereira Carvalho, W. S.; Jiang, Y.; Serpe, M. J. Portable Point-of-Care Diagnostic Devices. *Anal. Methods* **2016**, *8*, 7847−7867.
(7) Wang, X.; Cui, Q.; Yao, C.; Li, S.; Zhang, P.; Sun, H.; Lv, F.; Liu, L.; Li, L.; Wang, S. Conjugated Polyelectrolyte-Silver Nanostructure Pair for Detection and Killing of Bacteria. *Adv. Mater. Technol.* **2017**, *2*, 1700033.
(8) Zhu, S.; Wang, X.; Yang, Y.; Bai, H.; Cui, Q.; Sun, H.; Li, L.; Wang, S. Conjugated Polymer with Aggregation-Directed Intramolecular Förster Resonance Energy Transfer Enabling Efficient Discrimination and Killing of Microbial Pathogens. *Chem. Mater.* **2018**, *30*, 3244−3253.
(9) Hook, A. L.; Anderson, D. G.; Langer, R.; Williams, P.; Davies, M. C.; Alexander, M. R. High Throughput Methods Applied in Biomaterial Development and Discovery. *Biomaterials* **2010**, *31*, 187−198.
(10) Shapiro, E.; Biezuner, T.; Linnarsson, S. Single-Cell Sequencing-Based Technologies Will Revolutionize Whole-Organism Science. *Nat. Rev. Genet.* **2013**, *14*, 618−630.
(11) Aharoni, A.; Amitai, G.; Bernath, K.; Magdassi, S.; Tawfik, D. S. High-Throughput Screening of Enzyme Libraries: Thiolactonases Evolved by Fluorescence-Activated Sorting of Single Cells in Emulsion Compartments. *Chem. Biol.* **2005**, *12*, 1281−1289.
(12) Kamme, F.; Salunga, R.; Yu, J.; Tran, D.-T.; Zhu, J.; Luo, L.; Bittner, A.; Guo, H.-Q.; Miller, N.; Wan, J.; Erlander, M. Single-Cell Microarray Analysis in Hippocampus CA1_ Demonstration and Validation of Cellular Heterogeneity. *J. Neurosci.* **2003**, *23*, 3607−3615.
(13) Ueda, E.; Geyer, F. L.; Nedashkivska, V.; Levkin, P. A. Droplet Microarray: Facile Formation of Arrays of Microdroplets and Hydrogel Micropads for Cell Screening Applications. *Lab Chip* **2012**, *12*, 5218−5224.
(14) Ingham, C.; Bomer, J.; Sprenkels, A.; van den Berg, A.; de Vos, W.; van Hylckama Vlieg, J. High-Resolution Microcontact Printing and Transfer of Massive Arrays of Microorganisms on Planar and Compartmentalized Nanoporous Aluminium Oxide. *Lab Chip* **2010**, *10*, 1410−1416.
(15) Xu, L.; Robert, L.; Ouyang, Q.; Taddei, F.; Chen, Y.; Lindner, A. B.; Baigl, D. Microcontact Printing of Living Bacteria Arrays with Cellular Resolution. *Nano Lett.* **2007**, *7*, 2068−2072.
(16) Pepperkok, R.; Ellenberg, J. High-Throughput Fluorescence Microscopy for Systems Biology. *Nat. Rev. Mol. Cell Biol.* **2006**, *7*, 690−696.
(17) Grün, D.; van Oudenaarden, A. Design and Analysis of Single-Cell Sequencing Experiments. *Cell* **2015**, *163*, 799−810.
(18) Gawad, C.; Koh, W.; Quake, S. R. Single-Cell Genome Sequencing: Current State of the Science. *Nat. Rev. Genet.* **2016**, *17*, 175−188.
(19) Park, K. J.; Lee, K. G.; Seok, S.; Choi, B. G.; Lee, M. K.; Park, T. J.; Park, J. Y.; Kim, D. H.; Lee, S. J. Micropillar Arrays Enabling Single Microbial Cell Encapsulation in Hydrogels. *Lab Chip* **2014**, *14*, 1873−1879.
(20) Matsutani, A.; Takada, A. Single-Cell Isolation and Size Sieving Using Microenclosure Array for Microbial Analysis. *Sens. Mater.* **2015**, *27*, 383−390.
(21) Brouzes, E.; Medkova, M.; Savenelli, N.; Marran, D.; Twardowski, M.; Hutchison, J. B.; Rothberg, J. M.; Link, D. R.; Perrimon, N.; Samuels, M. L. Droplet Microfluidic Technology for

Single-Cell High-Throughput Screening. *Proc. Natl. Acad. Sci. U. S. A.* **2009**, *106*, 14195−14200.
(22) Mazutis, L.; Gilbert, J.; Ung, W. L.; Weitz, D. A.; Griffiths, A. D.; Heyman, J. A. Single-Cell Analysis and Sorting Using Droplet-Based Microfluidics. *Nat. Protoc.* **2013**, *8*, 870−891.
(23) Young, J. W.; Locke, J. C.; Altinok, A.; Rosenfeld, N.; Bacarian, T.; Swain, P. S.; Mjolsness, E.; Elowitz, M. B. Measuring Single-Cell Gene Expression Dynamics in Bacteria Using Fluorescence Time-Lapse Microscopy. *Nat. Protoc.* **2011**, *7*, 80−88.
(24) Van Manen, H. J.; Kraan, Y. M.; Roos, D.; Otto, C. Single-Cell Raman and Fluorescence Microscopy Reveal the Association of Lipid Bodies with Phagosomes in Leukocytes. *Proc. Natl. Acad. Sci. U. S. A.* **2005**, *102*, 10159−10164.
(25) Melamed, S.; Elad, T.; Belkin, S. Microbial Sensor Cell Arrays. *Curr. Opin. Biotechnol.* **2012**, *23*, 2−8.
(26) Anderson, D. G.; Putnam, D.; Lavik, E. B.; Mahmood, T. A.; Langer, R. Biomaterial Microarrays: Rapid, Microscale Screening of Polymer-Cell Interaction. *Biomaterials* **2005**, *26*, 4892−4897.
(27) Liu, C.; Liu, J.; Gao, D.; Ding, M.; Lin, J. M. Fabrication of Microwell Arrays Based on Two-Dimensional Ordered Polystyrene Microspheres for High-Throughput Single-Cell Analysis. *Anal. Chem.* **2010**, *82*, 9418−9424.
(28) Yamamura, S.; Kishi, H.; Tokimitsu, Y.; Kondo, S.; Honda, R.; Rao, S. R.; Omori, M.; Tamiya, E.; Muraguchi, A. Single-Cell Microarray for Analyzing Cellular Response. *Anal. Chem.* **2005**, *77*, 8050−8056.
(29) Park, S.; Kim, D.; Mitchell, R. J.; Kim, T. A Microfluidic Concentrator Array for Quantitative Predation Assays of Predatory Microbes. *Lab Chip* **2011**, *11*, 2916−2923.
(30) Pivetal, J.; Royet, D.; Ciuta, G.; Frenea-Robin, M.; Haddour, N.; Dempsey, N. M.; Dumas-Bouchiat, F.; Simonet, P. Micro-Magnet Arrays for Specific Single Bacterial Cell Positioning. *J. Magn. Magn. Mater.* **2015**, *380*, 72−77.
(31) Li, X.; Li, Z.; Xu, F.; Yan, Y.; Wang, W.; Li, L.; Liu, R.; Li, Z. Large-Scale Fabrication of Ordered Monolayer Self-Assembly of Polystyrene Submicron Spheres. *Appl. Sci.in Graphic Commun. Packaging* **2018**, *477*, 827−832.
(32) Chen, X.; Wei, X.; Jiang, K. Large-Scale Fabrication of Ordered Nanobowl Arrays. *Opt. Express* **2008**, *16*, 11888−11893.
(33) Li, H.; Ouyang, H.; Yu, M.; Wu, N.; Wang, X.; Jiang, W.; Liu, Z.; Tian, J.; Jin, Y.; Feng, H.; Fan, Y.; Li, Z. Thermo-Driven Evaporation Self-Assembly and Dynamic Analysis of Homocentric Carbon Nanotube Rings. *Small* **2017**, *13*, 1603642.
(34) Wang, X.; Summers, C. J.; Wang, Z. L. Large-Scale Hexagonal-Patterned Growth of Aligned ZnO Nanorods for Nano-Optoelectronics and Nanosensor Arrays. *Nano Lett.* **2004**, *4*, 423−426.
(35) Dudak, F. C.; Boyacı, İ. H. Development of An Immunosensor Based on Surface Plasmon Resonance for Enumeration of Escherichia coli in Water Samples. *Food Res. Int.* **2007**, *40*, 803−807.
(36) Lun, Z.-R.; Wang, Q.-P.; Chen, X.-G.; Li, A.-X.; Zhu, X.-Q. Streptococcus suis: An Emerging Zoonotic Pathogen. *Lancet Infect. Dis.* **2007**, *7*, 201−209.
(37) Moayeri, M.; Leppla, S. H.; Vrentas, C.; Pomerantsev, A. P.; Liu, S. Anthrax Pathogenesis. *Annu. Rev. Microbiol.* **2015**, *69*, 185−208.
(38) Wang, D.; Gao, Z.; Wang, H.; Feng, E.; Zhu, L.; Liu, X.; Wang, H. Curing Both Virulent Mega-Plasmids from Bacillus anthracis Wild-Type Strain A16 Simultaneously Using Plasmid Incompatibility. *J. Microbiol. Biotechnol.* **2015**, *25*, 1614−1620.
(39) Wang, X. Y.; Tao, F.; Xiao, D.; Lee, H.; Deen, J.; Gong, J.; Zhao, Y.; Zhou, W.; Li, W.; Shen, B.; Song, Y.; Ma, J.; Li, Z. M.; Wang, Z.; Su, P. Y.; Chang, N.; Xu, J. H.; Ouyang, P. Y.; von Seidlein, L.; Xu, Z. Y.; Clemens, J. D. Trend and Disease Burden of Bacillary Dysentery in China (1991-2000). *Bull. W. H. O.* **2006**, *84*, 561−568.
(40) Sarangi, B. R.; Gupta, M.; Doss, B. L.; Tissot, N.; Lam, F.; Mège, R.-M.; Borghi, N.; Ladoux, B. Coordination Between Intra- and Extracellular Forces Regulates Focal Adhesion Dynamics. *Nano Lett.* **2016**, *17*, 399−406.
(41) Gottenbos, B.; Grijpma, D. W.; Van der Mei, H. C.; Feijen, J.; Busscher, H. J. Antimicrobial Effects of Positively charged surfaces on adhering Gram-positive and Gram-negative bacteria. *J. Antimicrob. Chemother.* **2001**, *48*, 7−13.
(42) Wang, G.; Feng, H.; Hu, L.; Jin, W.; Hao, Q.; Gao, A.; Peng, X.; Li, W.; Wong, K.-Y.; Wang, H.; Li, Z.; Chu, P. K. An Antibacterial Platform Based on Capacitive Carbon-Doped TiO_2 Nanotubes After Direct or Alternating Current Charging. *Nat. Commun.* **2018**, *9*, 2055.
(43) Liu, B.; Ni, H.; Zhang, D.; Wang, D.; Fu, D.; Chen, H.; Gu, Z.; Zhao, X. Ultrasensitive Detection of Protein with Wide Linear Dynamic Range Based on Core-Shell SERS Nanotags and Photonic Crystal Beads. *ACS Sens.* **2017**, *2*, 1035−1043.
(44) Wang, D.; Ni, H.; Wang, Z.; Liu, B.; Chen, H.; Gu, Z.; Zhao, X. Discrimination of Nosiheptide Sources with Plasmonic Filters. *ACS Appl. Mater. Interfaces* **2017**, *9*, 13049−13055.
(45) Swider, C.; Maguire, K.; Rickenbach, M.; Montgomery, M.; Ducote, M. J.; Marhefka, C. A. Trace detection of meglumine and diatrizoate from Bacillus spore samples using liquid chromatography/mass spectrometry. *J. Forensic Sci.* **2012**, *57*, 923−931.
(46) Archer, N. K.; Mazaitis, M. J.; Costerton, J. W.; Leid, J. G.; Powers, M. E.; Shirtliff, M. E. Staphylococcus aureus biofilms: properties, regulation, and roles in human disease. *Virulence* **2011**, *2*, 445−459.

DOI: 10.1021/acsami.9b08662
ACS Appl. Mater. Interfaces 2019, 11, 44933−44940